Detection of powdery midiou in grapevine using remotely-sensed UV-induced fluorescence

M.C. Belanger, J.M. Roger, P. Cartolaro, A. Viau, Véronique Bellon Maurel

Detection of powdery mildew in grapevine using remotely-sensed UV-induced fluorescence.

M-C BÉLANGER [1], J-M ROGER [1], P. CARTOLARO[2], A. A. VIAU [3] and V. BELLON-MAUREL[1]

[1] UMR-ITAP, Cemagref, 361, rue Jean-François Breton, B.P. 5095, Montpellier, France, 34 196, cedex 5

[2] UMR Santé Végétale, INRA-ENITAB, Domaine de la Grande Ferrade,71, Avenue Edouard Bourlaux BP81, Villenave d'Ornon, France, 33883 cedex

[3] Laboratoire de Géomatique Agricole et Appliquée (GAAP), Pavillon Louis-Jacques-Casault, local 3731-A, Université Laval, Québec, G1K 7P4 Canada

Powdery mildew is caused by *Erysiphe necator* (syn. *Uncinula necator*), an ascomycete fungus. It can induce severe damage to a vineyard including yield loss and depreciation of wine sensory characteristics. This disease as other fungal diseases, is thoroughly controlled by pesticides. In order to reduce the use of pesticides and to improve early detection for this disease, we studied the potential of UV-induced imaging fluorescence to detect and quantify the colonisation of a leaf by *Erysiphe necator.* Cuttings of grapevine (*vitis vinifera* cv. Carbernet-Sauvignon) were grown in a greenhouse. Twenty-four leaves were collected and fourteen were inoculated with the fungus on their adaxial side, the remaining leaves were used as control. Images of fluorescence were taken in a

lab at six combinations of emission/$_{excitation}$ wavelength ($F440_{UV}$, $F520_{UV}$, $F690_{UV,}$ $F740_{UV}$, and $F690_{bl}$ $F740_{bl}$). Data treatments include proper image correction, interest area selection, fluorescence ratios computation and edge detection. Using the spatial average of fluorescence ratios for the whole leaf area it was possible to detect the fungus starting at 3 Days After Inoculation (DAI). Using the edge detection algorithm it was possible to detect and quantify the colonization of the leaf starting at 3 DAI, with a lower coefficient of variation compared to leaf spatial average.

Key words: *Erysiphe necator, vitis vinifera,* fluorescence, remote sensing, phytopathology, precision viticulture.

Introduction

The ascomycete fungus *Erysiphe necator* (syn. *Uncinula necator*), lives on the epidermal surface of green tissues and is responsible for the Powdery mildew on grapevine (Galet, 1976). In spring, the ascospores contained in the overwintering resistant cleistothecia are disseminated and they infect the grapevines. Powdery mildew can cause severe damage to a vineyard including yield loss and depreciation of wine sensory characteristics (Stummer et al., 2003; Stummer et al., 2005; Calonnec et al. 2004). Calonnec et al., (2004) have measured an average yield loss of 23.7 % of infested grapevine compared to healthy ones. The yield loss is accompanied by an increase in sugar content of 20 and 14 % for the diseased Cabernet Sauvignon and Sauvignon blanc berries, respectively, compared to healthy ones. A decrease in anthocyanin content for infested berries was also observed.

Currently, Powdery mildew such as other fungal diseases is thoroughly controlled by pesticides. In France, the vineyard production uses 20% of the nation's pesticides, including 30% of all fungicides (Aubertot et al., 2005) although it represents only 3% of the cultivated area (Agreste, 2006). The protection of crops against fungal attacks, mostly Downey and Powdery mildew raises a cost of nearly 360 euros per hectare (Aubertot et al., 2005). Integrated pest management is an alternative solution which could allow producers to reduce their use of pesticide from 30 to 50% (Aubertot et al., 2005). Without any operational model to forecast powdery mildew growth, the early detection of the infection points is necessary for an efficient implementation of Integrated Pest Management to control Powdery mildew. We suggest to use the optical

properties and more precisely the fluorescent properties of infected leaves to detect and quantify the fungal attack.

When an incompatible combination of host plant and fungi occurs, a hypersensitive response (HR) can be observed at the point of attack on the host plant or host cell (Agrios, 1988). On wheat plants, the HR resulted in a yellow colour autofluorescence (Zhang and Dickinson, 2001) and in a yellow-green colour autofluorescence in oat plants (Carver et al., 1998). The localized autofluorogens have been identified as being similar to phenolic compounds (Carver et al., 1998) although no evidence, such as the direct extraction and identification of phenolics from these microscopic, localized autofluorescent sites, exists. A normal expression of epidermal cell response to *Blumeria graminis* attack in oat, barley and wheat is localized autofluorescence (Carver et al., 1998). Mayama and Shishiyama, (1978) first described localized autofluorescence in barley epidermal cells attacked by *B. graminis* appressoria. For a compatible host/pathogen reaction as *Vitis vinifera/E. necator*, Ficke et al., (2004) observed a blue autofluorescence surrounding the appresoria on berries, indicating the localized accumulation of phenolic compounds. Not only infected plants fluoresce but also healthy plants. UV-induced plant fluorescence emits two types of fluorescence: blue-green fluorescence (BGF) and chlorophyll fluorescence (ChlF). Blue-green fluorescence is emitted at 440 and 520 nm mainly by ferulic acid that is present in cells walls of leaf veins and epidermis, therefore BGF mainly comes from leaf veins, petiole and stem (Cerovic et al., 1999). Chlorophyll fluorescence, on the other hand, comes mainly from leaf lamina and is emitted at 690 and 740 nm (Lichtenthaler, 1990). The relative intensities of BGF and ChlF are strongly

related to crop physiology and may provide additional data to secure the detection of powdery mildew.

The fungal structures themselves can also fluoresce; it was found that most rust (*Puccinia recondita* f sp. *tritici*) fungal structures fluoresced in bright blue without the use of fluorescent dye (Zhang and Dickinson, 2001).

Considering that new ways to achieve early detection of powdery mildew in grapevines would be very useful for Integrated Crop Protection, and that previous studies (Ficke et al., 2004; Zhang and Dickinson, 2001) indicated that UV-fluorescence could be a mean for such purpose, we evaluated if it was possible to detect powdery mildew (*Erysiphe necator*) on grapevine using remotely sensed imaging fluorescence. To do so, we collected fluorescence images on infected grapevine leaves and performed various data treatments to identify the one achieving the earliest and most efficient detection of *Erysiphe necator.* Thus this paper presents the methods used to create and process the fluorescence images and the resulting detection of powdery mildew.

Material & Methods

Plant material

Two experiments (A & B) took place respectively in 2005 & 2006. For both experiments, twelve grapevine cuttings (cv. Cabernet-Sauvignon) were grown in a greenhouse under a 16h photoperiod and controlled temperature (average 23°C day and 20°C night). The plants were kept free of powdery mildew by subliming sulphur for one hour, every night. On November 28th, 2005 for *exp. A* and on April 7th, 2006 for *exp. B*, twelve nearly mature leaves were collected from

grapevine plants at the rate of one leaf per plant. They were sterilized by immersing them 10 minutes in a solution of calcium hypochlorite (50g L^{-1}) then rinsed in distilled water and dried on sterilized filter paper. They were transferred to Petri dishes half filled with a neutral agar containing benzimidazole (30 mg L^{-1}). For *experiment A*, four leaves were infected on Nov 28th, four more on Nov 30th and the last four remained uninfected and were used as control leaves. For *experiment B*, six leaves were infected on April 7th and the last six remained uninfected and were used as control leaves. The infection was carried out by the *Institut National de Recherche Agronomique* (INRA) in Bordeaux, France with *Erysiphe necator* strain C3 for *exp. A* and S6 for *exp. B*. The Petri dishes containing the leaves to be infected were placed at the bottom of a Plexiglass tower having no lid. A diseased leaf (10 to 12 days after infection) was held over the Plexiglass tower and was air-sprayed in order to detach the conidia. Following air-transportation and gravity, the conidia were randomly distributed over the adaxial face of the leaves to be infected, resulting in a spore density of approximately 3 to 5 spores mm^{-2} (determined using a 40x Leica MZ6 binocular magnifier). The freshly infected leaves were kept unexposed to direct sunlight, in their closed Petri dish, in the lab, until fluorescence measurements. The period from infection to fluorescence measurement varied from 3 to 11 days after inoculation (DAI). The average room temperature was 22°C. The Nov 30th inoculation took place in a Cemagref Lab located in Montpellier, France. The inoculation setting was not exactly as the one used in Bordeaux and moreover, the inoculum spent a night in a cold room (< 10°C). Those conditions of conservation and inoculation may have compromised the

germination and sporulation of *Erysiphe necator* on the leaves infected on Nov. 30th.

Imaging fluorometer

Fluorescence measurements were realized using an imaging fluorometer presented in Belzile et al., (2003). The FLIM-100 imaging fluorometer used an interline CCD camera (CoolSnapHQ, RoperScientific, AZ, USA) modified for on-chip accumulation capability. The fluorescence was induced by a xenon flash lamp source (Hamamatsu, NJ, USA) producing intense light pulses at 50Hz repetition rate (4 μs pulse width) using a pulse generator (model 500B Berkeley Nucleonics Corporation, CA, USA). For plant leaf fluorescence applications, UV (360±40nm) and Blue (436±20nm) excitation wavelengths were selected using band pass filter (Chroma Technology Corp., VT, USA). The intensity of the excitation source varies according to the wavelength selected (0.04mW at 360 nm, 0.22mW at 440nm). The excitation pulses were synchronized with camera acquisition using proper electronics and control software. Image acquisition for each light pulse was done using 5 μs integration time. Charges were accumulated on a CCD side layer. The charges were transferred to the frame grabber at the end of image acquisition process. This system enabled gated detection of low light level signal without using an image intensifier. Fluorescence imaging requires between 75 to 2500 acquisitions depending on the sample and on detected wavelength. Four narrow band pass filters (CVI Laser, NM, USA) were placed in front of the camera allowing precise detection of 440, 520, 690 and 740 ± 10 nm

fluorescence. UV-induced fluorescence was measured at the four emission bands whereas blue-induced fluorescence intensities were measured at 690 and 740 nm. Plant leaf holder was 50 cm away from the excitation source thus effective fluorescence area was ~20 cm^2.

Fluorescence measurements

For fluorescence measurement, the leaves were extracted from the Petri dish using a pair of pliers. Distilled water was applied on the abaxial face to fix the leaf on the sample holder. Between each leaf, the sample holder was rinsed thoroughly using distilled water. All fluorescent measurements were done in a dark lab with all lights off, except for the excitation source. The leaves waiting for fluorescence measurements were kept on a window side.

Fluorescence measurements were done exactly 5, 7, 9, and 11 days after detachment (DAD) of the leaf from the plant for *exp. A* and 3, 5, and 7 DAD for *exp. B*. Thus corresponding to 5, 7, 9, and 11 days after inoculation (DAI) for the four leaves inoculated on November 28th, 2005 (herein referred to as x2811), to 3, 5, 7, and 9 DAI for the four leaves inoculated on November 30th, 2005 (herein referred to as x3011), to 3, 5, and 7 DAI for the six leaves inoculated on April 7th (herein referred to as x0704), and to zero DAI for the control plants.

Data treatment

In order to compare images from one fluorescence band to the others, proper image post-processing had to be made. Image correction (Eq. 1) was carried out according to non-uniformity of the light source, background signal, camera and

filter responsivity, and accumulations needed per acquisition. Light source non-uniformity correction was based on the light source normalized intensity pattern image (L, Eq.3) used to divide each raw image (I, Eq.2). Fluorescence images were then multiplied by responsivity factors (R) and divided by the number of accumulations needed (n) according to the detected wavelength. Figure 1 presents the spectral response of the detector and filters and the corresponding responsitivity factors.

$$F = \left(I \middle/ L \cdot R \right) \middle/ n \qquad [1]$$

where F =Corrected fluorescence image

I = raw fluorescence image

L = normalized light source intensity

R = the responsivity factors of the camera and filters at the selected wavelength, given by the manufacturers.

n = number of accumulations needed.

$$I = I_x - I_o \qquad [2]$$

where I is the raw fluorescence image; I_x and I_o are respectively the fluorescence images acquired with the excitation source on and off.

$$L = \left(L_x - L_o \right) \middle/ \max\left(L_x - L_o \right) \qquad [3]$$

where L is the normalized light source intensity; L_x and L_o are respectively the light source intensity images acquired at 440 nm on a white paper sheet with the UV-excitation source on and off, $\max\left(L_x - L_o \right)$ corresponds to the maximum.

For all fluorescence images, a mask was delineated to exclude non-leaf pixel for subsequent data treatment. The outline of the mask was delineated automatically using Matlab image processing toolbox (The Matworks, v 7.0,) and pixels inside the mask that had to be excluded were delineated manually. Once the mask was drawn, fluorescence ratios for each pixel and an average for the entire leaf were computed. The fluorescence ratios computed were F_{440}/F_{520}, F_{440}/F_{690}, F_{440}/F_{740}, F_{520}/F_{690}, F_{520}/F_{740}, F_{690}/F_{740}, UV epidermal transmittance measured at 690 nm (UV690) and at 740 nm (UV740) [Eq.4] (Bilger et al. 1997).

$$UV_{\lambda} = F_{\lambda UV} / F_{\lambda blue} \qquad [4]$$

where λ = the selected wavelength, either $690nm$ or $740nm$

$F_{\lambda UV}$ is the UV-induced fluorescence detected at $\lambda = 690nm$ or $740nm$

and $F_{\lambda blue}$ is the blue-induced fluorescence detected at $\lambda = 690nm$ or $740nm$

Figure 2 presents a schematic representation of the following data treatment. Once the fluorescence ratios were computed and the mask outlined, we computed the spatial average for each leaf area, resulting in one value per leaf for each date of measurements and each ratio. These values were used for the computation of the analysis of variance (ANOVA). The completely randomized ANOVA calculations were performed using the *glm* procedure from the SAS software (SAS Institute, NC, USA). This procedure uses the method of least squares to fit general linear models, it can relate one or several continuous dependent variables to one or several independent variables (SAS, 1999). In *experiment* A, because there was three treatments, we performed a contrast analysis to identify

the treatments significantly different from the control. This analysis computed a T-test under the custom hypothesis that the means of the first group equals the mean of the second one. For *experiment A* data, it resulted in two contrasts: one between control plants and the x2811 plants and one between control plants and the x3011 plants. The *exp. B* having only one treatment and the control, the computation of contrasts was not necessary. Parameters presenting heterogeneous variances were transformed using a logarithmic or Box-Cox transformation, the details concerning the Box-Cox transformation can be found in Peltier, (1998). Results are presented in Table 1.

For the following image analysis, we computed a megaimage for each fluorescence ratio at each date of measurement. As presented in Figure 3, a megaimage is computed by concatening n leaf images matrices (561 pixels * 761 pixels) to form a new and bigger image array ($561p$ pixels * $761q$ pixels) where $p*q=n$. The newly created mega image was saved in a TIFF format.

Using the megaimages formed for each fluorescence ratio, we determined a threshold of fluorescence intensity providing the best detection for the infected pixels. The thresholds were set using the last mega image taken (11 DAD for *exp. A* and 7 DAD for *exp. B*) and we compared the histograms curve of the infected leaves versus the control ones. We set the threshold at the crossing point of the two curves. Figure 4 presents the histograms of F_{440}/F_{520} from *exp. A* data and e*xp. B* data. Infected pixels have a fluorescence intensity value above the selected threshold. We applied the selected threshold to earlier images, for instance for exp. A, we developed the threshold on the 11 DAD image and we

applied it to the 5, 7, 9 and 11 DAD images. For exp. B. we developed the threshold on the 7 DAD image and applied it on the 3, 5 and 7 DAD fluorescence images. A different threshold was selected for each fluorescence ratio and it was then applied to each leaf, independently of the received treatment. For each leaf image we extracted the number of pixels having an intensity value above the selected threshold, we calculated the percent of infected area and then, we computed an ANOVA on this parameter using the SAS software as described previously. Results are presented in Table 2.

In addition to these data processing techniques we also tried to get benefit from the spatial heterogeneity between infected and control leaves. Indeed, the increase in fluorescence intensity observed at 440 and 520 nm is not uniformly distributed over the leaf surface. Even though the initial spore density is of 3 to 5 spore mm^{-2} it is very unlikely that the leaf surface be uniformly infected. The contamination of a leaf by *Erysiphe necator* starts with a conidia and the mycelium grows exclusively on the leaf surface following in an erratic way a radial pattern around the infection point (Peros et al. 2006). Thus, an image processing algorithm detecting the edge pattern is more likely to detect significant differences between treatments than an unsupervised image classification method. Image analysis was carried out based on an edge detection algorithm on each image of raw fluorescence data using the *canny* algorithm in the Image processing toolbox of Matlab (The Matworks, v 7.0,). The *canny* algorithm sets up two different thresholds in order to detect strong and weak edges, and includes the weak edges in the output only if they are connected to strong edges. For each image we extracted the number of *edge* pixels and we

computed an ANOVA on this parameter using the SAS software as described above. Results are presented in Table 3.

Results and discussion

Plants and fungal material

Figure 5 shows digital colour RGB pictures of *exp. A* infected and uninfected grapevine leaves taken from a) orthogonal view, b) side view and c) through a binocular. Figure 5 shows that the powdery mildew is hardly detected by the human eye especially when the axis of view is orthogonal to the leaf surface. When the pictures are taken from the side, the mycelium and conidiophores of *Erysiphe necator* are more likely to be detected, especially because the conidiophores, *i.e.* the structure holding the conidia, grow perpendicular to the leaf surface.

Fluorescence images

Fluorescence images clearly show the development of *Erysiphe necator* over the leaf surface of grapevine plants. Figure 6 presents the images of UV-induced fluorescence collected at different wavelengths (440 nm, 520 nm and F_{690}/F_{740}) on four different leaves taken from *exp. A* and *B* at 3 and 5 DAI. The fluorescence detected at 440 nm clearly shows the growth of the fungus over the leaf surface by an increase in fluorescence intensity, punctually at first and then along leaf veins and surface. At first, only spots of increased intensity are noticeable (3 DAI) then the leaf surface is gradually covered (x2811 and then x0704). To a lesser extent, the same distribution pattern can also be detected at 520 nm, although the detected spots are not as clearly defined as they were in F_{440}.

F_{690}/F_{740} does not present significant visual differences between control leaves and the infected ones.

For all the data presented in the tables 1 to 3, the reader will notice a major difference between the detection of powdery mildew achieved on x2811 and x0704 compared to x3011. In general, it is possible to detect the powdery mildew on x3011 leaves but later than on x2811 or x0704. As said earlier, x3011 inoculation was performed in a different lab under different conditions than those prevailing during x2811 and x0704 inoculations. The diseased leaf used to inoculate x3011 spent a night in a cold room and it might have reduced the germination rate of the conidia.

Spatial average of fluorescence ratios

Based on standard data treatment for fluorescence measurements, we computed for each leaf, a spatial average of each fluorescence ratio. Table 1 presents the means of spatial average of fluorescence ratios for all treatments at all corresponding dates of measurements. Although the two experiments were generated the same way there are some differences in the values presented in Table 1. Data from *exp.A* are generally lower than the ones from *exp.B* except for F_{440}/F_{520} and F_{690}/F_{740}, that are similar and for UV690 and UV740 that are higher. As presented earlier, plant fluorescence is strongly related to crop physiology. Based on earlier work on various crops, researchers have observed an increase in F_{440}/F_{690}, F_{440}/F_{740}, F_{520}/F_{690}, and F_{520}/F_{740} in response to nitrogen deficiency (Belanger, 2005; Heisel et al., 1996) and an increase in BGF/ChlF resulting from leaf ageing (Cartelat et al. 2005; Meyer et al. 2003). The nitrogen

deficiency and leaf ageing also reduce the epidermal transmittance to UV rays (UV690 and UV740) (Apostol el al., 2003; Samson et al., 2000, Cartelat et al. 2005; Meyer et al. 2003). Those results suggest that there was a significant difference between *exp. B* and *A*, either on nutrition or leaf age. For this reason, the reader should always compare x0704 leaves with their corresponding control data, that has been submitted to the same stress. The response of x0704 to powdery mildew will be reflected in the changes observed between x0704 and its control.

Now considering the powdery mildew effects, there is a significant increase in F_{440}/F_{520} starting at 7 DAI for x2811 and 3 DAI for x0704. Starting at 9 DAI for x2811 and 3 DAI for x0704, there was a significant increase in F_{440}/F_{690}. Compared to control leaves, a significant increase in F_{440}/F_{740} is detected starting at 5 DAI for x0704 and it is nearly significant starting at 9 DAI for both x2811 and x3011. Those increases are due to the increase in fluorescence detected at 440 nm compared to the fluorescence emitted at 690 and 740 nm, which seems to be less affected by the fungus presence. There is a significant change observed in F_{690}/F_{740} for x3011 but there is no related changes in previous or subsequent measurements. No significant changes were observed for F_{520}/F_{690}, F_{520}/F_{740}, UV_{690}, and UV_{740} for all treatments compared to control plants.

According to our results, the powdery mildew could be detected in less than 10 DAI and as soon as 3 DAI for x0704, especially using F_{440}/F_{520}. An early detection could increase the efficiency of pesticide applications either by timely application or by inclusion in an integrated pest management. Early detection through fluorescence measurements could also be used as an indicator for the

application of bio control agents. Recently, Melidossian et al., (2005) published a study in which they evaluate the efficiency of a mycophageous mite to suppress *Erysiphe necator*. Their in-field and in-lab results were very satisfactory, especially if the treatment was applied 1 day before and up to 10 days after inoculation. This treatment could eventually be used in combination with a detection unit based on fluorescence measurements.

Image analysis

In order to measure the leaf area where there is an increase in fluorescence intensity, we determined a threshold for delineating the infected pixels from the healthy ones. Table 2 presents the ratio of infected pixels over healthy ones using this method. The selected thresholds (I) are also identified. Thresholds used on *exp. A* data were determined using the image histogram of *exp. A*. The thresholds used on *exp. B* data were determined using the images histograms of *exp. B*. In *exp. A*, it is possible to detect a significant ($p<0.05$) difference between healthy pixels and infected ones using F_{440}/F_{520} starting at 7 DAI for x2811 and 5 DAI for x3011. For F_{440}/F_{690} a significant increase is detected starting 11 DAI for x2811. For F_{440}/F_{740} the method presented in Table 2 can detect a significant difference earlier than the averaged intensity of leaf fluorescence presented in Table 1 but only for the *exp. B* treatments. F_{440}/F_{520} data from control leaves (Table 2, *exp. A*) show a reduction in the proportion of pixels having an intensity >126. It may be due to leaf deterioration, indeed leaves were detached from the plant for as long as 11 days. This effect is not observed on *exp. B* data whose leaves were detached for a maximum of 7 days.

For F_{440}/F_{520} the threshold selection resulted in similar threshold selected compared to *exp.A* data In *exp. B*, it is possible to detect a significant ($p<0.05$) difference between healthy pixels and infected ones using F_{440}/F_{520} starting at 3 DAI. For F_{440}/F_{690} and F_{440}/F_{740} a significant increase is detected starting at 5 DAI. There were no detection made using F_{520}/F_{690}, F_{520}/F_{740} and F_{690}/F_{740} and only punctual detection ($p<0.1$) were achieved using UV690 and UV740.

Using only one rule of decision such as a threshold may not be sufficient. The detection of powdery mildew would probably be more efficient if more decision rules were integrated.

Data obtained by the threshold method show a large coefficient of variation (CV). For instance, CV is 46 % for control leaves, 23 % for x2811, 46 % for x3011 and 31 % for x0704. when the corresponding threshold is applied over F_{440}/F_{520} data

The edge detection algorithm was computed over all fluorescence images (not computed as ratios). The figure 7 presents the edge detection process in two steps: 1) the raw image, 2) the edges detected on F_{440} images for two *exp. A* leaves, taken 9 DAD. One can see that the severity of the infection is reflected in the number of edge detected that is larger in x2811(9 DAI) than in the control. The Table 3 presents the ratio of edge pixels detected over the whole leaf pixels (%). Using the F_{440} images, a significant increase in the number of edges is detected starting at 5 DAI for x2811, at 9 DAI for x3011 and at 3 DAI for x0704. Significant differences are also detected using F_{520} starting at 3 DAI for x0704 only.

Data generated using the edge detection algorithm show a reduction in coefficient of variation (CV) compared to the threshold method presented in Table 2. CV is

now of 19 % for control leaves, 16 % for x2811, 29 % for x3011 and 11 % for x0704.

Erysiphe necator as other fungal disease has a radial growth pattern that can be observe on the leaf surface. Taking advantage of this characteristic development, the edge detection algorithm can achieve a more reliable detection than the threshold method.

Conclusion

The results obtained here show that it is possible to remotely detect *Erysiphe necator* especially when using the F_{440} images or the F_{440}/F_{520} fluorescence ratio. The advantage of using F_{440}/F_{520} instead of F_{440}/F_{690} or F_{440}/F_{740} is that the F_{440}/F_{520} ratio is much less sensitive to short-term physiological stresses than the F_{440}/F_{690} and F_{440}/F_{740} ratios (Buschmann and Lichtenthaler, 1998). Various long-term stress conditions often yield to considerably lower values of F_{440}/F_{520} (Buschmann and Lichtenthaler, 1998) contrary to the increase in F_{440}/F_{520} observed following the induction of a fungal attack in our study.

It is possible to achieve the detection of *Erysiphe necator* and moreover, the quantification of its growth over a leaf surface. This is useful to estimate the power of actual defence tools or to develop new means of defence against the fungus.

Under natural growth conditions, *Erysiphe necator* infection is more likely to start on the abaxial side of a leaf. Therefore, the best detection should be achieved by measuring fluorescence on the abaxial side of the leaf, using for instance, a handheld device. In order to collect data in a more efficient way, the

use of remote sensing has to be planned. Large field areas are usually scanned using airborne or tractor-mounted sensors. Those sensors aim at the canopy capturing mostly views of the adaxial side of the leaves. It would be interesting to test if it is possible to detect the presence of the fungus from the adaxial side. Using a handheld or an airborne device, a regionalized detection of *Erysiphe necator* could yield to a localized treatment including either integrated pest management, pest control by fungicides or proper preventive control applied in a determined radius around the detected infection point.

Acknowledgements : The authors wish to thank Dr. Olivier Naud and Dr. Agnès Calonnec for their scientific advices and appreciated collaboration.

REFERENCES

Agreste., 2006. Statistique agricole annuelle. [Online]. Available by Ministère de l'agriculture et de la pêche (France) http://agreste.agriculture.gouv.fr/enquetes_3/statistique_agricole_annuelle_60/index.html (verified 2006-05-12).

Agrios, G.N., 1988. Plant Pathology, 3rd Edition, Academic Press, San Diego, CA, USA. 803 p.

Apostol, S., Viau, A.A., Tremblay, N., Briantais, J.-M., Prasher, S., Parent, L.-E. and Moya, I., 2003. Laser induced fluorescence signatures as a tool for remote monitoring of water and nitrogen stresses in plants. Canadian journal of remote sensing 29:57-65.

Aubertot, J.N., Barbier, J.M., Carpentier, A., Gril, J.J., Guichard, L., Lucas, P., Savary, S., Savini, I. and Voltz, M., 2005. Pesticides, agriculture et environnement. Réduire l'utilisation des pesticides et limiter leurs impacts environnementaux. [Online]. Available by INRA et Cemagref http://www.inra.fr/l_institut/missions_et_strategie/les_missions_de_l_inra/eclairer_les_decisions/pesticides_rapport_d_expertise (verified 2006-03-21).

Belanger, M.-C., 2005. Détection de carences nutritives par fluorescence active et spectrométrie. Ph.D. thesis, Université Laval, Qc.Canada. 202 p. [Online] Available by Université Laval http://www.theses.ulaval.ca/2005/22913/22913.pdf

Belzile, C., Bélanger, M.-C. , Viau, A.A., Chamberland, M. and Roy, S., 2003. An operational system for crop assessment, p. 244-252, *In* B. S. Bennedsen, et al., eds. Proceedings of Photonic East conference: Monitoring Food Safety, Agriculture, and Plant Health, Vol. 5271. SPIE, Providence, RI.

Bilger, W., Veit, M., Schreiber, L., and Schreiber, U. 1997. Measurement of leaf epidermal transmittance of UV radiation by chlorophyll fluorescence. Physiologia plantarum 101:754-763.

Buschmann, C. and Lichtenthaler, H.K., 1998. Principles and characteristics of multicolour fluorescence imaging of plants. Journal of Plant Physiology 152:297-314.

Calonnec, A., Cartolaro, P., Poupot, C., Dubourdieu, D. and Darriet, P., 2004. Effects of *Uncinula necator* on the yield and quality of grapes (*Vitis vinifera*) and wine. Plant pathology 53:434-445.

Cartelat, A., Cerovic, Z.G., Goulas, Y., Meyer, S., Lelarge, C., Prioul, J-L., Barbottin, A., Jeuffroy, M-H., Gate, P., Agati, G., Moya, I. 2005. Optically assessed contents of leaf polyphenolics and chlorophyll as indicators of nitrogen deficiency in wheat (*Triticum aestivum*, L.) Field Crops Research, vol. 91, pp.35-49.

Carver, T.L.W., Thomas, B.J., Robbins, M.P. and Zeyen, R.J., 1998. Phenylalanine ammonia-lyase inhibition, autofluorescence, and localized accumulation of silicon calcium and manganese in oat epidermis attacked by the powdery mildew fungus *blumeria graminis*(DC) Speer. Physiological and molecular plant pathology 52:223-243.

Cerovic, Z.G., Samson, G., Morales, F., Tremblay, N. and Moya, I., 1999. Ultraviolet-induced fluorescence for plant monitoring: present state and prospects. Agronomie 19:543-578.

Ficke, A., Gadoury, D.M., Seem, R.C., Godfrey, D. and Dry, I.B., 2004. Host barrier and responses to *Uncinula necator* in developing grape berries. Phytopathology 94:438-445.

Galet, P., 1976. Précis de viticulture. 3rd ed., Montpellier, France.

Lichtenthaler, H.K., 1990. Applications of chlorophyll fluorescence in stress physiology and remote sensing, p. 287-305, *In* M. D. Steven and J. A. Clark, eds. Applications of remote sensing in agriculture. Butterworhs Publisher.

Mayama, S. and Shishiyama, J., 1978. Localized accumulation of fluorescent and UV-absorbing compounds at penetration sites in barley leaves infected with *Erysiphe graminis hordei*. Physiological plant pathology 13:347-354.

Melidossian, H.S., Seem, R.C., English-Loeb, G., Wilcox, W.F. and Gadoury, D.M., 2005. Suppression of grapevine powdery mildew by a mycophagous mite. Plant disease 89:1331-1338.

Meyer, S., Cartelat, A., Moya, I., and Cerovic, Z.G. 2003. UV-induced blue-green and far-red fluorescence along wheat leaves: a potential signature of leaf ageing. Journal of experimental botany, vol. 54, no.383, pp.757-769.

Peltier, M.R., Wilcox, C.J. and Sharp, D.C., 1998. Technical Note: Application of the Box-Cox Data Transformation to animal science experiments. Journal of animal science, vol. 76, pp.847-849.

Péros, J.P., Nguyen, T.H., Troulet, C., Michel-Romiti, C., and Notteghem, J.L. 2006. Assessment of powdery mildew resistance of grape and Erysiphe necator pathogenicity using a laboratory assay. Vitis 45:29-36.

Samson, G., Tremblay, N., Dudelzak, A.E., Babichenko, S.M., Dextrase, L. and Wollring, J., 2000. Nutrient stress of corn plants: early detection and discrimination using a compact multiwavelength fluorescent lidar, p. 214-223 4th EARSeL Workshop Lidar Remote Sensing of Land and Sea, Vol. 1, Dresden, Germany.

SAS, 1999. SAS/STAT User's Guide, The GLM Procedure. [Online] Available by SAS Institue at http://v8doc.sas.com/sashtml/

Stummer, B.L., Francis, L., Markides, A.J. and Scott, E.S., 2003. The effect of powdery mildew infection on grape berries and wine composition and sensory properties of Chardonnay wines. Australian Journal of grape and wine research 9:28-39.

Stummer, B.L., Francis, I.L., Zanker, T., Lattey, K.A. and Scott, E.S., 2005. Effects of powdery mildew on the sensory properties and composition of Chardonnay juice and wine when grape sugar ripeness is standardised. Australian Journal of grape and wine research 11:66-76.

Zhang, L. and Dickinson, M., 2001. Fluorescence from rust fungi: a simple and effective method to monitor the dynamics of fungal growth *in planta*. Physiological and molecular plant pathology 59:137-141.

Table 1: Means of spatial averages of fluorescence ratios for the three treatments, taken at different dates, for *exp. A* and *exp. B* data. DAD=Days after detachment and DAI= Days after inoculation. x2811 and x0704 where inoculated on the day they were detached so DAI=DAD but for x3011: DAI=DAD-2.

Ratio	*Exp. A*			*Exp. B*	
Date of measure	Control	x2811	x3011	Control	x0704
F_{440}/F_{520}					
3 DAD	n.a.	n.a.	n.a.	0.501	**0.788 *****
5 DAD	0.544	0.617	**0.337 ****	0.526	**1.124 *****
7 DAD	0.519	**0.703 ****	0.544	0.537	**0.964 *****
9 DAD	0.534	**0.853 *****	0.598	n.a.	n.a.
11 DAD	0.440	**0.716 *****	**0.650 *****	n.a.	n.a.
F_{440}/F_{690}					
3 DAD	n.a.	n.a.	n.a.	0.046	**0.097 ****
5 DAD	0.018	0.019	0.011	0.058	**0.139 *****
7 DAD	0.019	0.024	0.018	0.053	**0.127 *****
9 DAD	0.019	**0.032 ****	0.023	n.a.	n.a.
11 DAD	0.015	**0.026 ****	0.021	n.a.	n.a.
F_{440}/F_{740}					
3 DAD	n.a.	n.a.	n.a.	0.053	0.081
5 DAD	0.016	0.017	0.009	0.059	**0.154 *****
7 DAD	0.017	0.024	0.016	0.054	**0.121 *****
9 DAD	0.021	**0.031 ***	0.020	n.a.	n.a.
11 DAD	0.014	**0.026 ***	**0.030 ***	n.a.	n.a.
F_{520}/F_{690}					
3 DAD	n.a.	n.a.	n.a.	0.094	0.111
5 DAD	0.032	0.028	0.026	0.106	0.121
7 DAD	0.033	0.034	0.032	0.096	0.132 *
9 DAD	0.034	0.037	0.035	n.a.	n.a.
11 DAD	0.033	0.036	0.028	n.a.	n.a.
F_{520}/F_{740}					
3 DAD	n.a.	n.a.	n.a.	0.102	0.101
5 DAD	0.030	0.026	0.029	0.107	0.131
7 DAD	0.031	0.034	0.028	0.094	0.123 *
9 DAD	0.036	0.036	0.032	n.a.	n.a.
11 DAD	0.030	0.036	0.031	n.a.	n.a.
F_{690}/F_{740}					
3 DAD	n.a.	n.a.	n.a.	1.119	0.975
5 DAD	0.963	0.943	1.025	1.116	1.207
7 DAD	0.951	**0.999 ***	**0.889 ****	1.016	0.955
9 DAD	1.084	0.976	0.934	n.a.	n.a.
11 DAD	0.957	1.001	1.063	n.a.	n.a.
UV_{690}					
3 DAD	n.a.	n.a.	n.a.	0.091	0.090
5 DAD	0.303	0.329	0.396	0.086	0.096
7 DAD	0.312	0.342	0.345	0.091	0.089
9 DAD	0.297	0.334	0.310	n.a.	n.a.
11 DAD	0.289	0.342	0.322	n.a.	n.a.
UV_{740}					
3 DAD	n.a.	n.a.	n.a.	0.110	0.108
5 DAD	0.351	0.356	0.391	0.101	0.113
7 DAD	0.379	0.379	0.412	0.112	0.112
9 DAD	0.293	0.392	0.392	n.a.	n.a.
11 DAD	0.359	0.399	0.396	n.a.	n.a.

n.a.= data not available

***, **, * = significant at respectively $p<0.01$, $p<0.05$, and $p<0.10$.

Table 2: Means of infested areas over healthy ones (%) determined using the presented threshold on fluorescence images taken at different dates, for *exp. A* and *exp. B* data DAD=Days after detachment and DAI= Days after inoculation. x2811 and x0704 where inoculated on the day they were detached so DAI=DAD but for x3011: DAI=DAD-2.

Ratio						
	threshold	Control	x2811	x3011	Control	x0704
Date of measure		----------%----------			- ----------%----------	
F_{440}/F_{520}	**(I>126) [1]**				**(I>144) [2]**	
3DAD		n.a.	n.a.	n.a.	13.81	**48.06 *** **
5 DAD		43.39	52.79	45.77	10.36	**95.47 *** **
7 DAD		22.77	**67.67 *** **	**39.68 ** **	13.06	**88.06 *** **
9 DAD		32.36	**78.44 *** **	**50.28 ** **	n.a.	n.a.
11 DAD		9.99	**87.61 *** **	**66.20 *** **	n.a.	n.a.
F_{440}/F_{690}	**(I>3) [1]**				**(I>16) [2]**	
3 DAD		n.a.	n.a.	n.a.	16.26	42.72
5 DAD		49.54	63.12	60.75	11.17	**85.88 *** **
7 DAD		41.53	66.04	54.85	9.06	**86.72 *** **
9 DAD		46.32	**96.68 * **	59.10	n.a.	n.a.
11 DAD		31.72	**93.85 ** **	**38.27 * **	n.a.	n.a.
F_{440}/F_{740}	**(I>4) [1]**				**(I>14) [2]**	
3 DAD		n.a.	n.a.	n.a.	20.98	46.82
5 DAD		24.02	26.18	5.62	13.27	**87.48 *** **
7 DAD		13.76	49.88	16.81	9.45	**88.87 *** **
9 DAD		19.57	**84.84 *** **	**30.36 *** **	n.a.	n.a.
11 DAD		12.06	**66.44 *** **	**19.23 *** **	n.a.	n.a.
F_{520}/F_{690}	**(I>8) [1]**				**(I>40) [2]**	
3 DAD		n.a.	n.a.	n.a.	12.13	16.71
5 DAD		33.85	36.74	82.32	8.73	29.02
7 DAD		32.22	42.27	41.84	6.35	31.28
9 DAD		31.44	51.69	42.32	n.a.	n.a.
11 DAD		31.96	47.88	8.308	n.a.	n.a.
F_{520}/F_{740}	**(I>8) [1]**				**(I>34) [2]**	
3 DAD		n.a.	n.a.	n.a.	19.68	21.32
5 DAD		26.92	26.11	41.40	12.09	32.43
7 DAD		25.16	41.65	26.24	7.84	34.39
9 DAD		24.55	46.81	30.26	n.a.	n.a.
11 DAD		24.93	43.85	7.77	n.a.	n.a.
F_{690}/F_{740}	**(I>230) [1]**				**(n.d.) [2]**	
3 DAD		n.a.	n.a.	n.a.		
5 DAD		33.83	39.21	**13.20 *** **		
7 DAD		34.68	37.16	25.41		
9 DAD		27.63	**42.17 ** **	**31.33 * **	n.a.	n.a.
11 DAD		31.18	36.73	40.57	n.a.	n.a.
UV_{690}	**(I>83) [1]**				**(I<11 et I>21) [2]**	
3 DAD		n.a.	n.a.	n.a.	42.87	**76.46 * **
5 DAD		43.02	51.47	8.07	39.26	64.09
7 DAD		42.18	33.41	52.02	40.22	59.52
9 DAD		37.96	50.11	37.25	n.a.	n.a.
11 DAD		26.87	50.97	75.89	n.a.	n.a.
UV_{740}	**(I>118) [1]**				**(I<16 et I>28) [2]**	
3 DAD		n.a.	n.a.	n.a.	36.12	**67.94 * **
5 DAD		7.96	54.29	2.71	34.29	60.97
7 DAD		31.81	7.53	33.73	33.66	**66.17 * **
9 DAD		9.03	24.22	28.85	n.a.	n.a.
11 DAD		8.98	25.79	55.22	n.a.	n.a.

***, **, * = significant at respectively p<0.01, p<0.05, and p<0.10.

[1, 2] threshold determined respectively on *exp. A* and *exp B* megaimage and I= fluorescence intensity

Table 3: Means of infected pixels over healthy ones (%) as detected by the edge detection method on UV-induced fluorescence images taken at four wavelength, for the two experiments, at different dates. DAD=Days after detachment and DAI= Days after inoculation. x2811 and x0704 where inoculated on the day they were detached so DAI=DAD but for x3011: DAI=DAD-2.

Fluorescence Intensity					
	Control	x2811	x3011	Control	x0704
Date of measure	----------	%	----------	----------	% ----------
F_{440}					
3 DAD	n.a.	n.a.	n.a.	11.74	**19.14 *****
5 DAD	7.09	**15.27 *****	8.55	8.71	**21.09 *****
7 DAD	8.15	**16.57 *****	9.93	7.06	**18.42 *****
9 DAD	8.33	**18.08 *****	11.95	n.a.	n.a.
11 DAD	8.48	**17.15 *****	**13.65 *****	n.a.	n.a.
F_{520}					
3 DAD	n.a.	n.a.	n.a.	15.72	**19.79 ****
5 DAD	14.14	15.87	13.71	15.89	**20.97 *****
7 DAD	14.99	17.34	14.98	14.95	**18.86 ****
9 DAD	15.57	17.15	15.26	n.a.	n.a.
11 DAD	14.92	16.25	15.62	n.a.	n.a.
F_{690}					
3 DAD	n.a.	n.a.	n.a.	19.53	20.35
5 DAD	21.02	19.59	21.26	19.40	19.81
7 DAD	21.27	21.12	21.28	19.34	20.62 *
9 DAD	21.12	20.63	20.68	n.a.	n.a.
11 DAD	20.75	20.81	20.91	n.a.	n.a.
F_{740}					
3 DAD	n.a.	n.a.	n.a.	18.83	18.73
5 DAD	19.36	20.36	21.55	18.87	18.29
7 DAD	20.64	20.02	20.90	18.44	19.16
9 DAD	20.12	20.52	20.75	n.a.	n.a.
11 DAD	20.01	19.77	19.41	n.a.	n.a.

n.a.=data not available

***, **, * = significant at respectively $p<0.01$, $p<0.05$, and $p<0.10$.

Figures captions

Figure 1: a) spectral response of the camera and filters and b) responsivity factors.

Figure 2: Schematic representation of data treatment and statistical analysis

Figure 3: Megaimage composition

Figure 4: Threshold selection, on 11 DAD F_{440}/F_{520} image histograms from *exp. A* and on 7 DAD F_{440}/F_{520} image histograms from *exp.B.* Infected pixels have a fluorescence intensity (I) value above the selected threshold.

Figure 5: The grapevine leaves in their Petri dishes 11 DAD from, a) top view, b) side view and c) through a binocular of a control plant, x2811 which is a leaf inoculated on Nov.28th (11 DAI) and x3011 which has been inoculated on Nov. 30th (9 DAI).

Figure 6: UV-induced fluorescence images a) F440 taken 3 Days After Inoculation (DAI), b) F440 taken 5 DAI, c) F520 taken 3 DAI, d) F520 taken 5 DAI, e) F690/F740 taken 3 DAI and f) F690/F740 taken 5 DAI.

Figure 7: Edge detection examples on F_{440} fluorescence images: a) F_{440} image of a control plant (9 DAD), b) edges detected on the control plant (9 DAD) using the canny algorithm, c) F_{440} image of a x2811 plant (9 DAI), and d) b) edges detected on the x2811 plant (9 DAI) using the canny algorithm. DAD = days after detachment and DAI= days after inoculation.

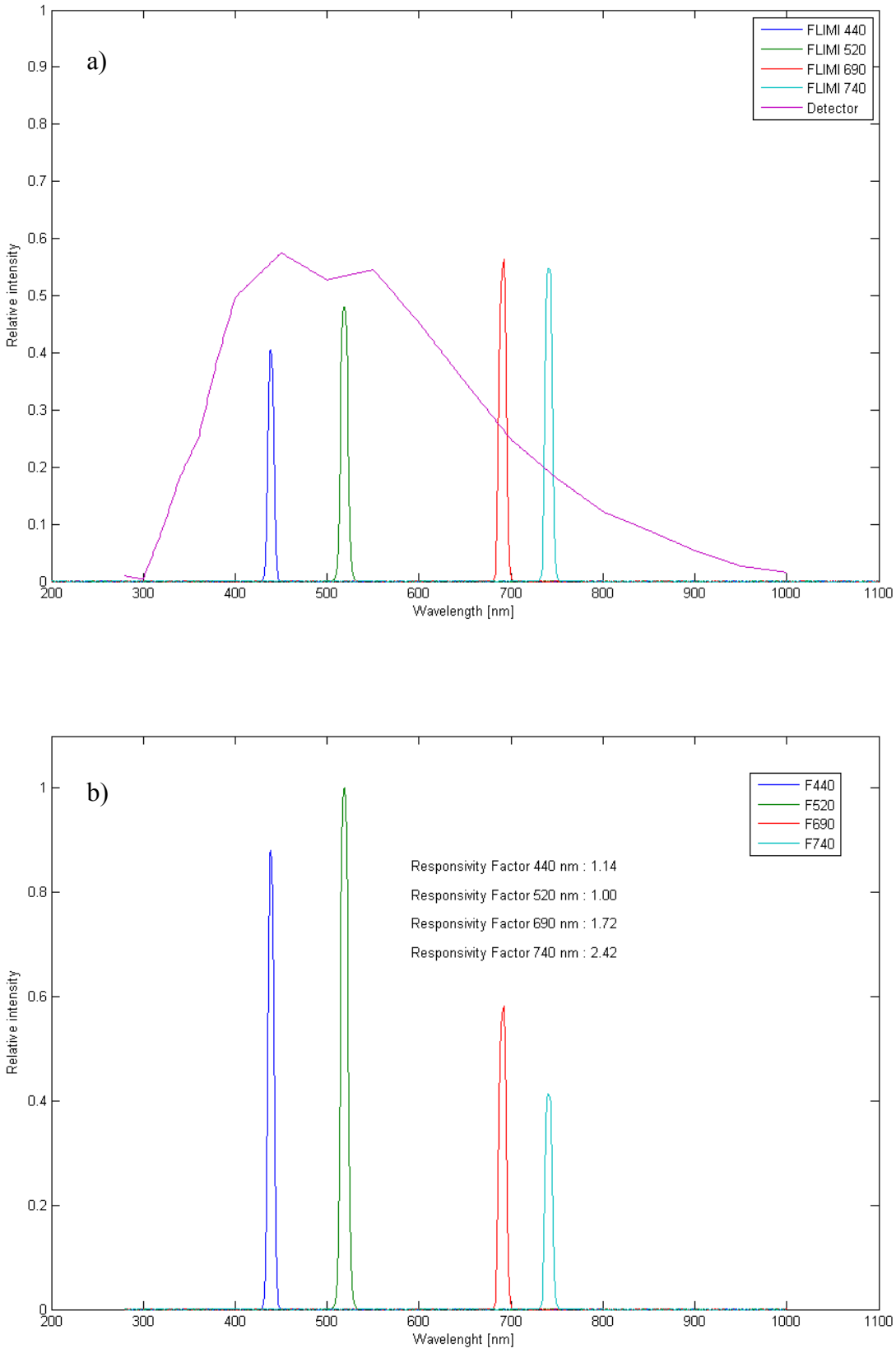
a)
FLIMI 440
FLIMI 520
FLIMI 690
FLIMI 740
Detector
Relative intensity
Wavelength [nm]
b)
F440
F520
F690
F740
Responsivity Factor 440 nm : 1.14
Responsivity Factor 520 nm : 1.00
Responsivity Factor 690 nm : 1.72
Responsivity Factor 740 nm : 2.42
Relative intensity
Wavelenght [nm]

Figure 1

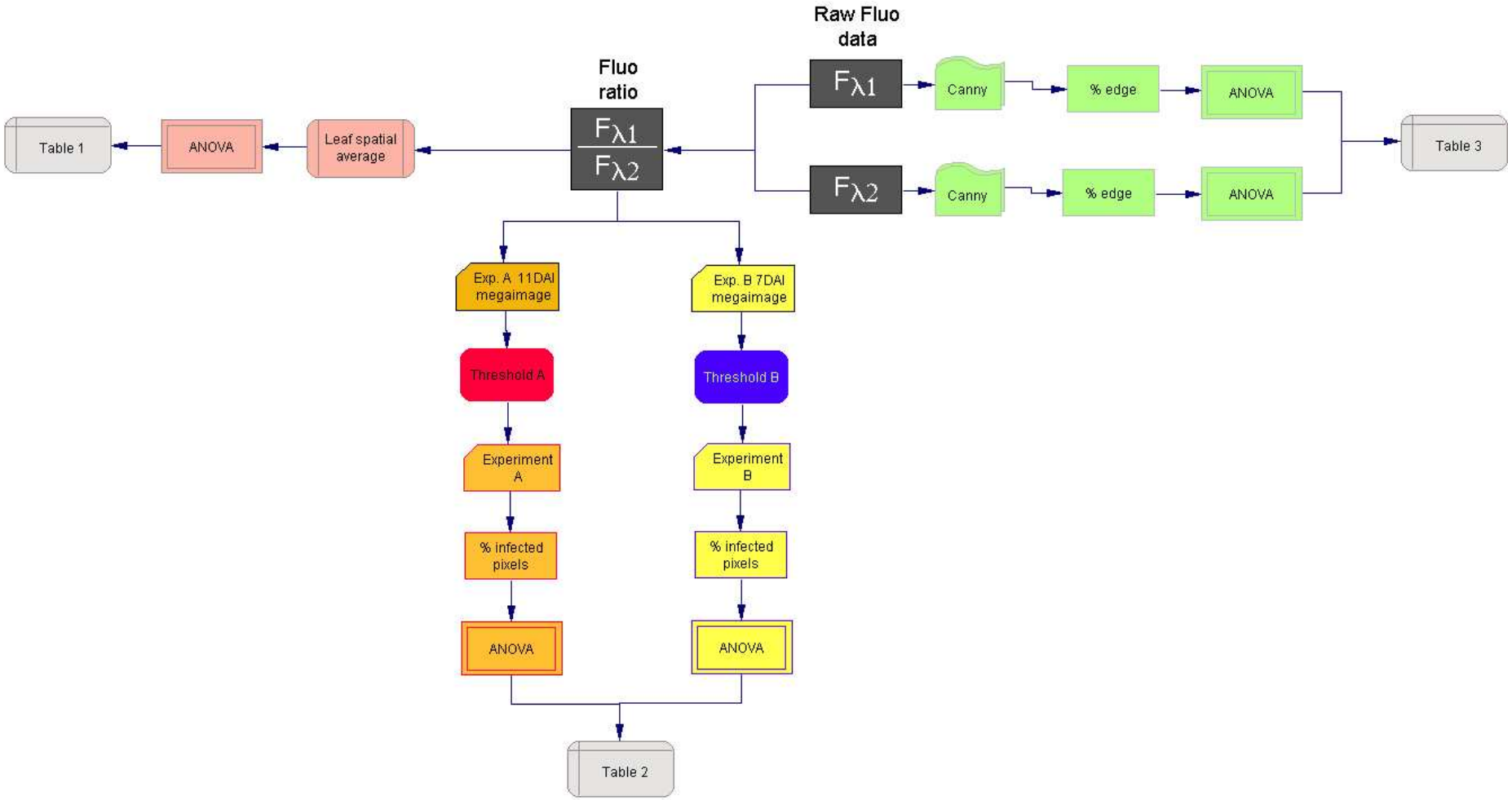
Raw Fluo data
Fluo ratio
Fλ1
Fλ2
Canny
% edge
ANOVA
Table 3
Table 1
ANOVA
Leaf spatial average
Exp. A 11DAI megaimage
Exp. B 7DAI megaimage
Threshold A
Threshold B
Experiment A
Experiment B
% infected pixels
Table 2
For each leaf image, average of pixels values over all the leaf surface.
Leaf spatial average
Edge detection using the Canny algorithm provided in Matlab Image processing Toolbox
Canny
Combination of all single leaf images into one bigger image. One megaimage is computed for each fluorescence ratio at each date of measurements.
Megaimage
The threshold is selected by superposing the the infected and control leaves megaimage histograms and visually identifying the cutoff. Red is done using experiment A data and blue using experiment B data
Threshold A

Figure 2

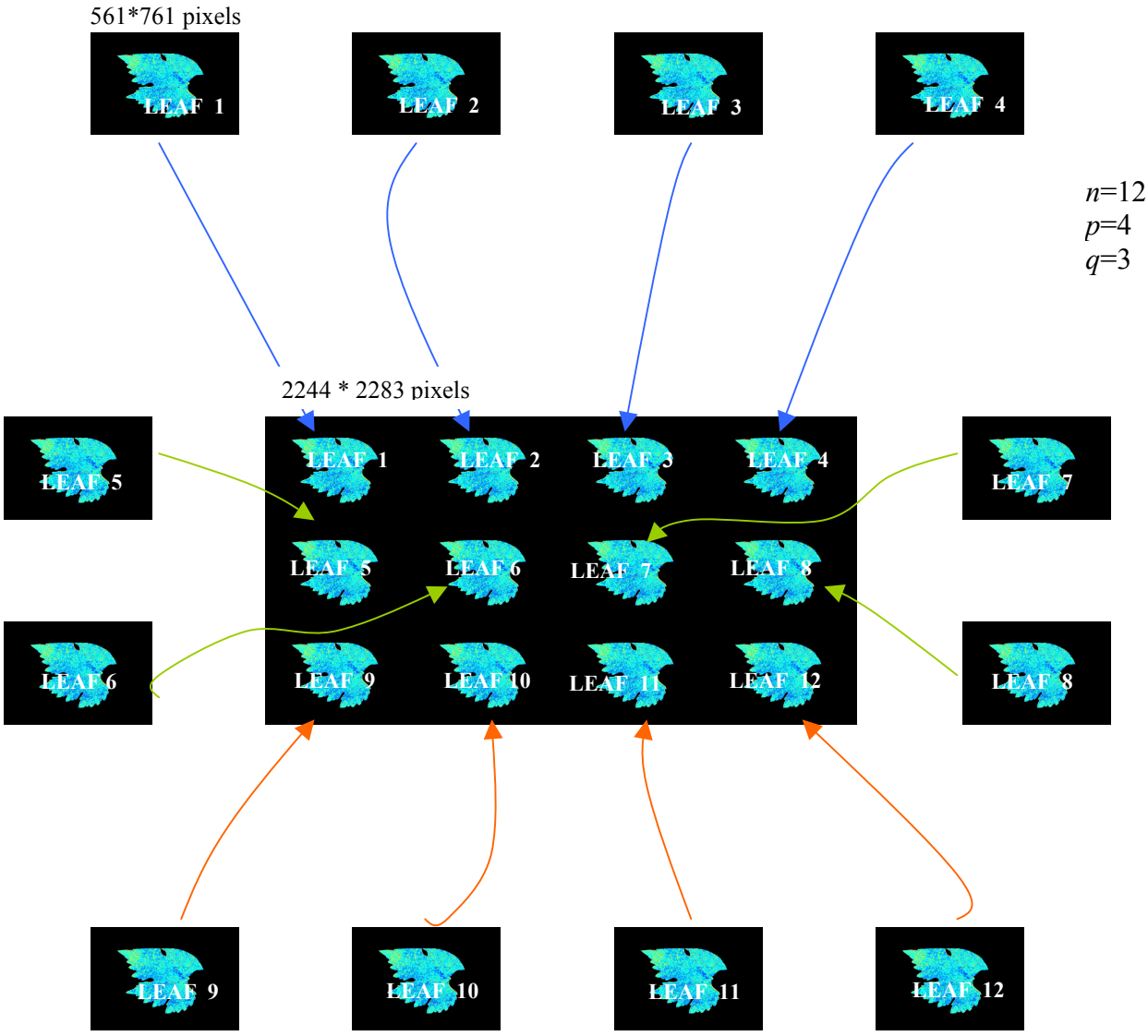

Figure 3
Megaimage composition

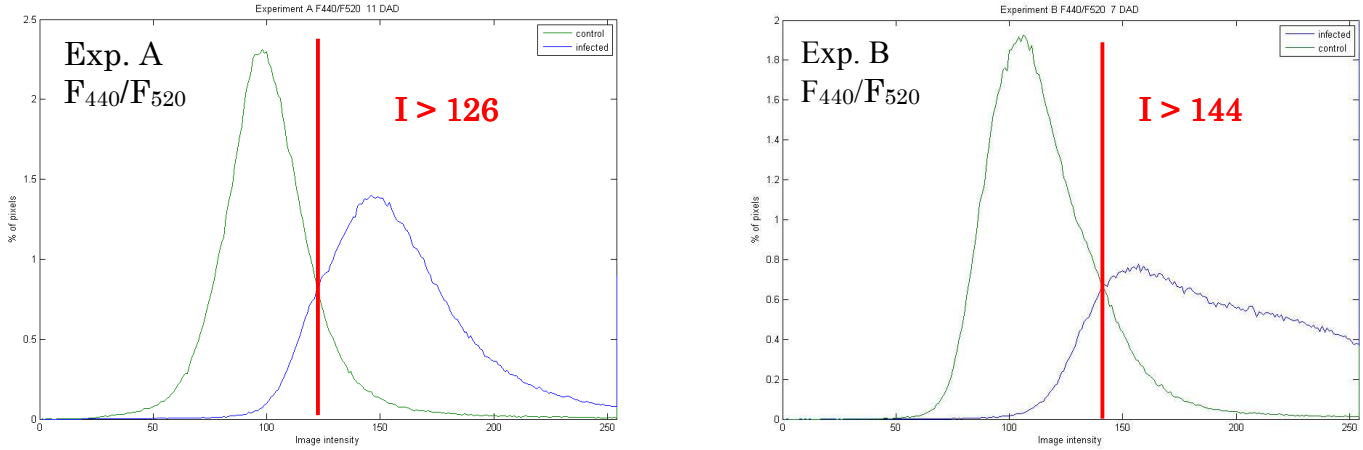
Experiment A F440/F520 11 DAD
Exp. A
F440/F520
I > 126
control
infected
% of pixels
Image intensity
Experiment B F440/F520 7 DAD
Exp. B
F440/F520
I > 144
infected
control
% of pixels
Image intensity

Figure 4

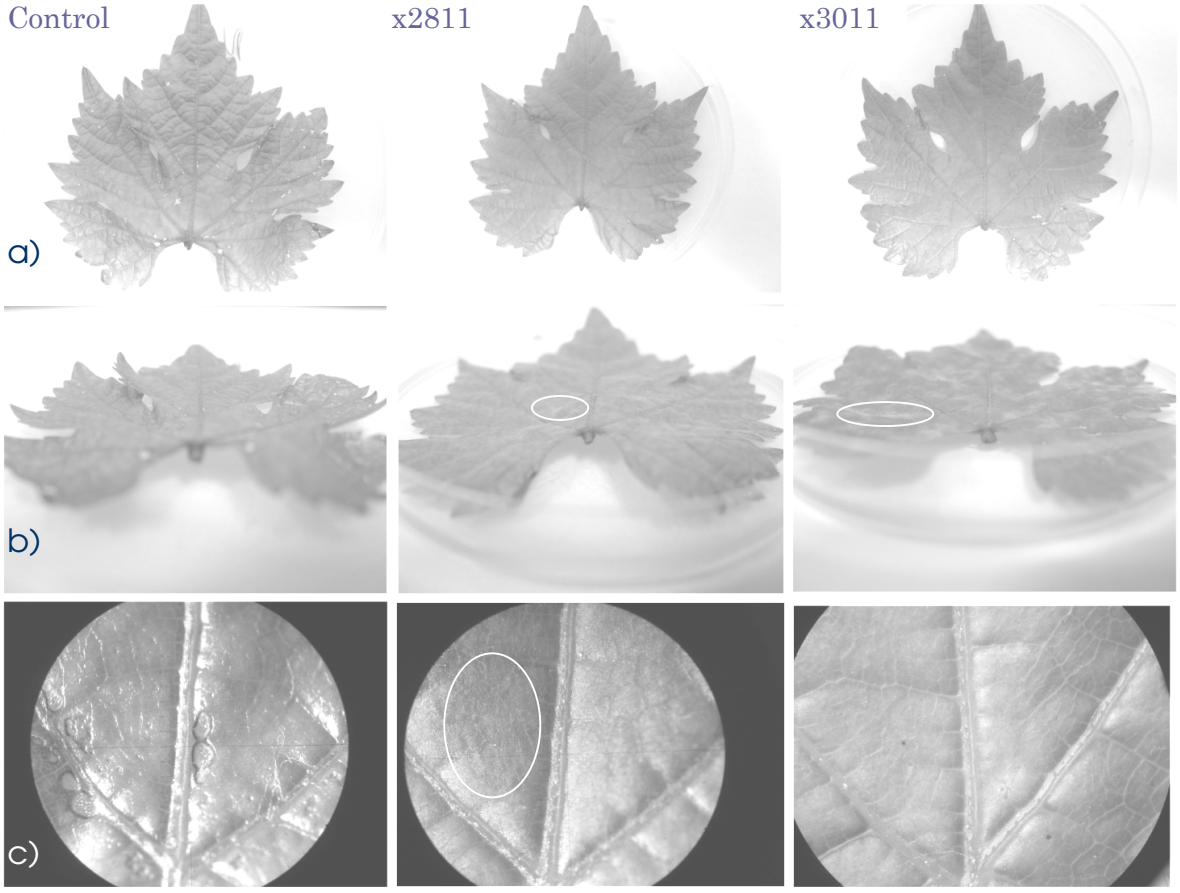

Figure 5

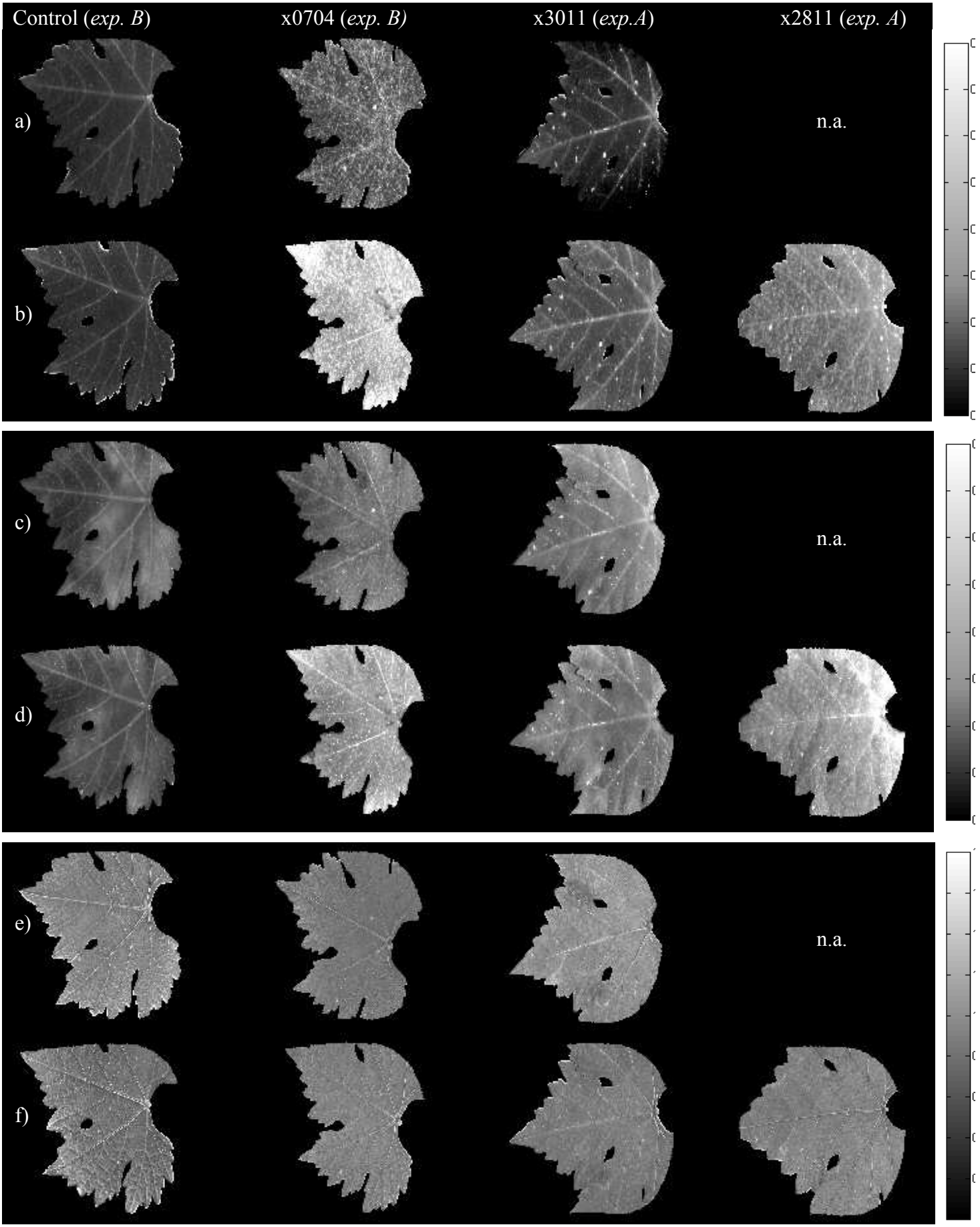
Control (*exp. B*)
x0704 (*exp. B)*
x3011 (*exp.A*)
x2811 (*exp. A*)
a)
n.a.
b)
c)
n.a.
d)
e)
n.a.
f)

Figure 6

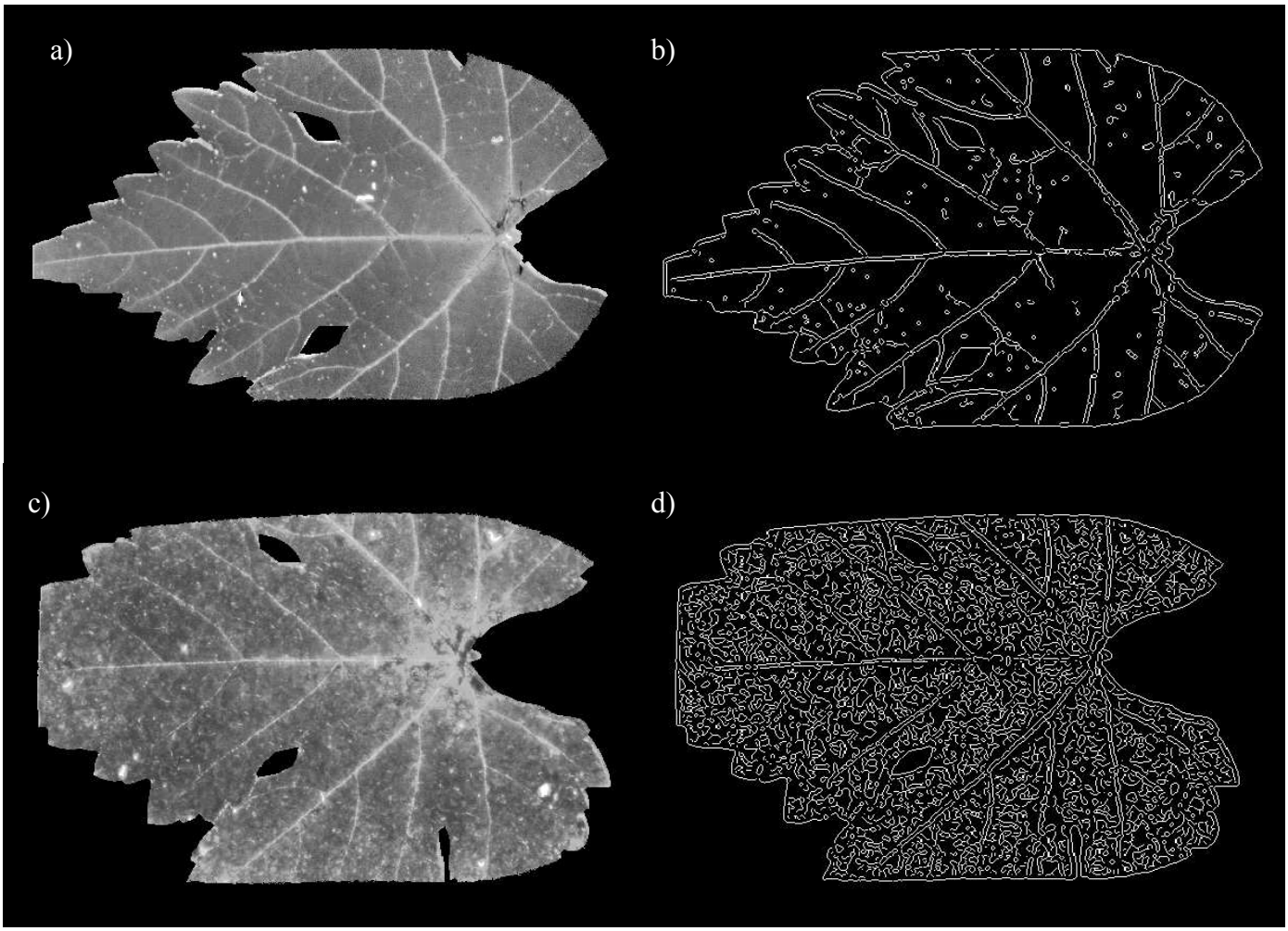

Figure 7